



Received 14 April 2025

Accepted 23 April 2025

Edited by W. T. A. Harrison, University of
Aberdeen, United Kingdom**Keywords:** crystal structure; 4-aminoantipyrine;
aerial oxidation; dimethylformamide; hydrogen
bonding; Hirshfeld surface.**CCDC reference:** 2446090**Supporting information:** this article has
supporting information at journals.iucr.org/e

Structure of (*E*)-4-amino-5-[[[(1,5-dimethyl-3-oxo-2-phenyl-2,3-dihydro-1*H*-pyrazol-4-yl)imino]methyl]-1-methyl-2-phenyl-2,3-dihydro-1*H*-pyrazol-3-one: aerial oxidation of 4-aminoantipyrine in dimethylformamide

R. Kumaravel,^a Helen Stoeckli-Evans,^{b*} A. Subashini,^{c*} M. G. Shankar,^{c,d} Monika Kučeráková,^e Michal Dušek,^e Aurélien Crochet^f and K. Ramamurthi^g

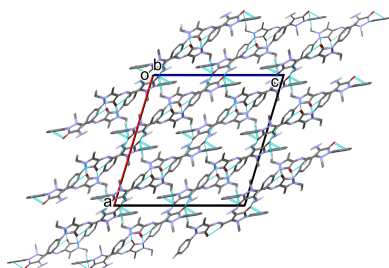
^aDepartment of Physics, Annapoorana Engineering College (Autonomous), Salem - 636308, Tamilnadu, India, ^bInstitute of Physics, University of Neuchâtel, Rue Emile-Argand 11, CH-2000 Neuchâtel, Switzerland, ^cPG and Research Department of Physics, Srimad Andavan Arts and Science College (Autonomous), Affiliated to Bharathidasan University, Tiruchirappalli - 620005, Tamilnadu, India, ^dDepartment of Physics, Swami Dayananda College of Arts and Science, Affiliated to Bharathidasan University, Manjakudi - 612610, Tamilnadu, India, ^eInstitute of Physics ASCR, Na Slovance 2, 182 21 Praha 8, Czech Republic, ^fChemistry Department, University of Fribourg, Chemin du Musée 9, CH-1700 Fribourg, Switzerland, and ^gCrystal Growth and Thin Film Laboratory, Department of Physics, Bharathidasan University, Tiruchirappalli - 620024, Tamilnadu, India. *Correspondence e-mail: helen.stoeckli-evans@unine.ch, viji.suba@gmail.com

The title compound, C₂₂H₂₂N₆O₂ (**I**), is the result of the aerial oxidation of the 5-methyl group of 4-aminoantipyrine to an aldehyde group followed by Schiff base formation with a second molecule of 4-aminoantipyrine. The reaction only takes place in the presence of dimethylformamide. The central unit of the molecule is close to planar, the pyrazole rings being inclined to each other by 3.74 (15)°. There is an intramolecular N—H···N hydrogen bond enclosing an *S*(6) ring motif and there are two further *S*(6) rings involving weak C—H···O=C hydrogen bonds. The molecule has an *E* configuration about the azomethine (—N=CH—) bond. In the crystal, inversion-related molecules are linked by pairs of N—H···O hydrogen bonds, forming dimers enclosing *R*₂²(10) loops. The dimers are linked by C—H···O hydrogen bonds and C—H··· π interactions, leading to the formation of a three-dimensional supramolecular network.

1. Chemical context

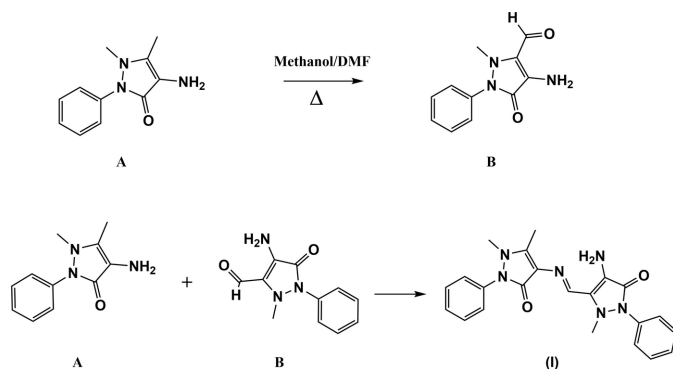
The crystal structure of 4-aminoantipyrine (4-amino-1,5-dimethyl-2-phenyl-1,2-dihydro-3*H*-pyrazol-3-one, C₁₁H₁₃N₃O or ampyrone or 4-AAP) has been reported by Li *et al.* (2013) and by Mnguni & Lemmerer (2015), and a co-crystal of 4-AAP has been reported on by Smith & Lemmerer (2019). The crystal structure of 4-(*N,N*-dimethyl)-aminoantipyrine was described by Singh & Vijayan (1976). Derivatives of 4-AAP account for at least two pharmaceutical drugs, aminoantipyrine and 4-(*N,N*-dimethyl)-aminoantipyrine, both of which have been used as analgesics for over a century.

The formation of the title compound, (**I**), is best explained by the aerial oxidation of the 5-methyl group of 4-AAP to an aldehyde group, forming 4-amino-2-methyl-5-oxo-1-phenyl-2,5-dihydro-1*H*-pyrazole-3-carbaldehyde and subsequent Schiff base formation with a second molecule of 4-aminoantipyrine. The reactivity of the methyl group is indicated by the hyperconjugative effect and oxidation to the aldehyde by air takes place in the presence of dimethylformamide (DMF). The role of DMF in chemistry has been reviewed by Heravi *et*



Published under a CC BY 4.0 licence

al. (2018). They noted that DMF has been used as a reagent in a number of important organic reactions, such as the Vilsmeier–Haack reaction (Vilsmeier & Haack, 1927), which result in the formylation of hetero-aromatic compounds



Compound **(I)** was produced serendipitously when attempts were made to form CdCl_2 or HgCl_2 complexes of 4-aminoantipyrene (Stoekli-Evans *et al.*, 2025), when dimethylformamide (DMF) was added to the reaction mixture. When the reaction was repeated in various solvents in the absence of the metal halide, for example with methanol and acetonitrile or methanol and acetone, no reaction took place. It was found that compound **(I)** was only formed when DMF was present as one of the solvents.

To the best of our knowledge, the aerial oxidation of an aminoantipyrene was first reported by Kametani *et al.* (1967). A yellow substance was formed as a byproduct when studying the fusion of 4-(*N,N*-dimethyl)-aminoantipyrene with barbituric acid in the presence of air. To obtain a large amount of this yellow compound the reaction was repeated by introducing air into a heated solution of the aminoantipyrene in different solvents, such as ethanol, acetic acid or acetic anhydride. They showed by NMR and IR spectroscopic analyses that they had produced the aldehyde, 4-(dimethylamino)-2-methyl-5-oxo-1-phenyl-2,5-dihydro-1*H*-pyrazole-3-carbaldehyde (Kametani *et al.*, 1967).

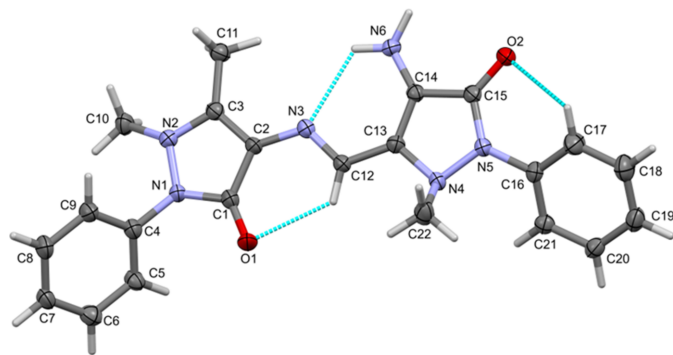


Figure 1
A view of the molecular structure of **(I)** with atom labelling and displacement ellipsoids drawn at the 50% probability level.

Table 1
Hydrogen-bond geometry (\AA , $^\circ$).

Cg1 is the centroid of C4–C9 phenyl ring.

$D-H\cdots A$	$D-H$	$H\cdots A$	$D\cdots A$	$D-H\cdots A$
$\text{N6}-\text{H6AN}\cdots\text{N3}$	0.90 (4)	2.30 (4)	2.894 (3)	123 (3)
$\text{N6}-\text{H6BN}\cdots\text{O2}^{\text{i}}$	0.98 (3)	2.09 (3)	2.953 (3)	147 (3)
$\text{C7}-\text{H7}\cdots\text{O2}^{\text{ii}}$	0.95	2.49	3.417 (4)	165
$\text{C10}-\text{H10D}\cdots\text{O2}^{\text{iii}}$	0.98	2.52	3.472 (4)	164
$\text{C12}-\text{H12}\cdots\text{O1}$	0.95	2.34	3.022 (3)	128
$\text{C17}-\text{H17}\cdots\text{O2}$	0.95	2.55	3.013 (4)	110
$\text{C11}-\text{H11B}\cdots\text{Cg1}^{\text{iii}}$	0.98	2.96	3.645 (3)	128

Symmetry codes: (i) $-x+1, -y+1, -z+1$; (ii) $x-\frac{1}{2}, -y+\frac{3}{2}, z+\frac{1}{2}$; (iii) $x, -y+1, z+\frac{1}{2}$.

The result of aerial oxidation of the 5-methyl group of certain 4-aminoantipyrene Schiff bases to form *in situ* $-\text{CH}_2\text{OH}$, $-\text{CH}(\text{OH})_2$ and $-\text{COOH}$ groups has been observed in the formation of various copper(II) and cobalt(II) complexes (see §4. Database survey).

2. Structural commentary

The molecular structure of **(I)** is illustrated in Fig. 1. The central unit is close to planar with the pyrazole rings, N1/N2/C1–C3 (r.m.s. deviation = 0.036 \AA) and N4/N5/C13–C15 (r.m.s. deviation = 0.035 \AA), being inclined to each other by 3.74 (15) $^\circ$. The planarity of the central unit is consolidated by the presence of an intramolecular $\text{N6}-\text{H6AN}\cdots\text{N3}$ hydrogen bond (Table 1), which generates an $S(6)$ ring motif, as do two $\text{C}-\text{H}\cdots\text{O}=\text{C}$ hydrogen bonds (Table 1 and Fig. 1).

The title molecule has an *E* configuration about the azomethine ($-\text{N3}=\text{C12H}-$) bond whose bond length is 1.297 (3) \AA . This is slightly longer than the average value of 1.286 (6) \AA (see §4. Database survey). The arene ring C4–C9 is inclined to the pyrazole ring N1/N2/C1–C3 mean plane by 55.63 (14) $^\circ$, while the arene ring C16–C21 is inclined to the pyrazole ring N4/N5/C13–C15 mean plane by 32.84 (15) $^\circ$. The arene rings are inclined to each other by 44.19 (4) $^\circ$.

The sum of the angles subtended by the methyl substituted atom N2 is 354.9 $^\circ$. In contrast, the methyl-substituted N atom, N4, has a definite pyramidal geometry with the corresponding sum of angles being 328.8 $^\circ$. This later value is more typical and is similar to the value of 332.4 $^\circ$ reported for 4-AAP (CSD refcode LOYXEE; Mnguni & Lemmerer, 2015). See also §4. Database survey.

3. Supramolecular features

In the crystal of **(I)**, inversion-related molecules are linked by pairwise $\text{N}-\text{H}\cdots\text{O}$ hydrogen bonds, forming dimers enclosing an $R_2^2(10)$ ring motif (Table 1, Fig. 2). The dimers are linked by $\text{C}-\text{H}\cdots\text{O}$ hydrogen bonds and $\text{C}-\text{H}\cdots\pi$ interactions (Table 1), forming a three-dimensional supramolecular network (Fig. 3).

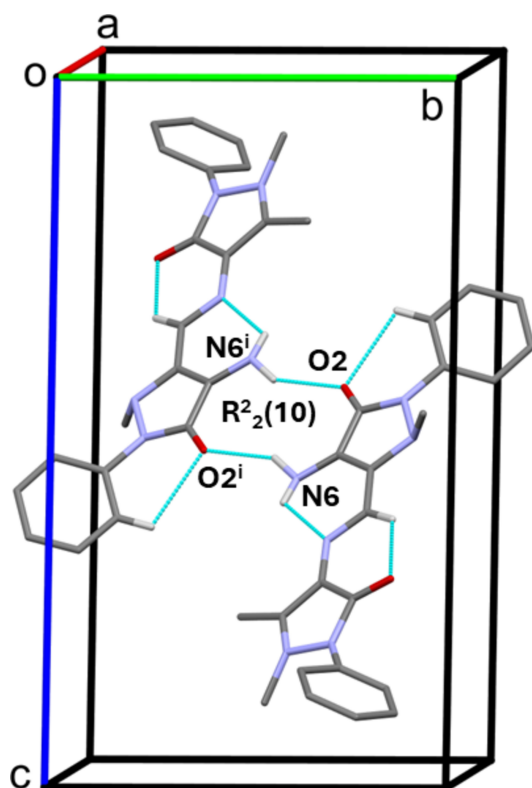


Figure 2
A partial view along the *a* axis of the crystal packing of (**I**). Inversion-related molecules are linked by a pair of N–H...O hydrogen bonds (Table 1), forming a dimer enclosing an $R^2_2(10)$ ring motif.

4. Database survey

A search of the Cambridge Structural Database (CSD, V5.46 update February 2025; Groom *et al.*, 2016) for the 4-AAP moiety gave 582 hits; 413 are organic compounds and 169 are metal–organic complexes. In a series of copper(II) and cobalt(II) complexes, *in situ* oxidation of the 5-methyl group of the pyrazole moiety takes place. For the copper(II)

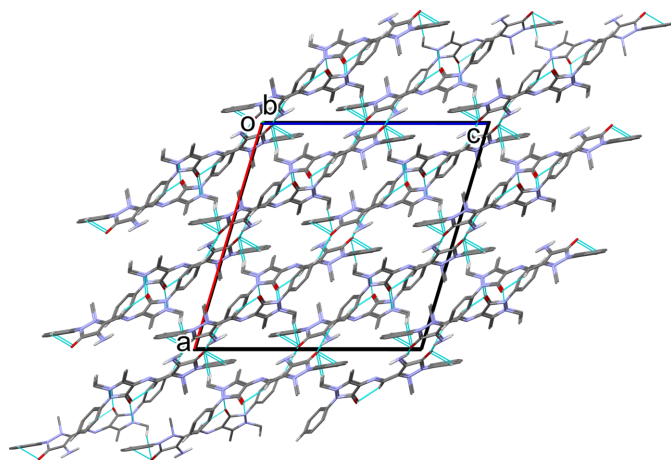


Figure 3
A view along the *b* axis of the crystal packing of (**I**). For clarity, only the H atoms involved in hydrogen bonding (Table 1) have been included.

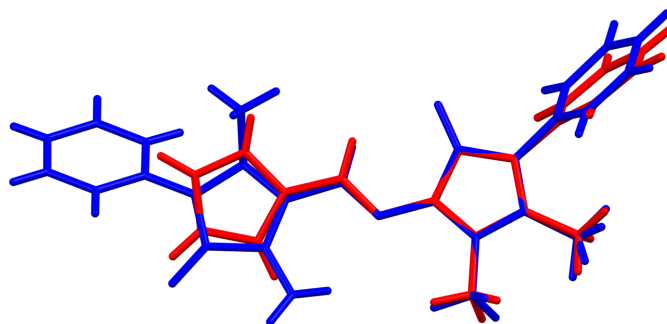


Figure 4
A view of the structural overlay of (**I**) and DEXTAC (Jing & Chen, 2007); the r.m.s. deviation is 0.018 Å (*Mercury*; Macrae *et al.*, 2020).

complexes (CSD refcodes: CIHPUF; Wang & Zheng, 2007 and JAXSOU; Parvarinezhad *et al.*, 2022) the transformation is to an alcohol ($-\text{CH}_2\text{OH}$). For the cobalt(II) complexes three transformations have been observed, to $-\text{CH}_2\text{OH}$, $-\text{CH}(\text{OH})_2$ and $-\text{COOH}$ (CSD refcodes: JUNMAI, JUNMEM and JUNMIQ; Loukopoulos *et al.*, 2015). Full details and references of the CSD search are given in the supporting information.

A search of the CSD for Schiff base derivatives of 4-AAP with an $-\text{N}=\text{C}-$ bond (with the following restrictions: three-dimensional coordinates determined, *R* factor ≤ 0.075 , no disorder, no errors, not polymeric, no ions, single crystals only and only organics) yielded 208 hits. The analysis in *Mercury* (Macrae *et al.*, 2020) of the $-\text{N}=\text{C}-$ bond length found that it varies from 1.256 to 1.300 Å, with a mean value of 1.282 (6) Å. In (**I**) the N3=C12 bond length is slightly longer at 1.297 (3) Å. The dihedral angles involving the phenyl ring and the mean plane of the pyrazole ring vary from 32.4 to 80.2°, with an average value of 52.32 (15)°. As noted above, the corresponding values observed for the two 4-AAP moieties in (**I**) are 55.63 (14) and 32.84 (15)°, the latter dihedral angle being close to the lower limit value.

The pyramidal geometry of the methyl-substituted N atom of the pyrazole ring, measured by the sum of the three angles involving the N atom, was found to have a lower limit of *ca* 340° in the two independent molecules of 4-((*E*)-{2-[*N*-(1,5-dimethyl-3-oxo-2-phenyl-2,3-dihydro-1*H*-pyrazol-4-yl)-carboximidoyl]benzylidene}amino)-1,5-dimethyl-2-phenyl-2,3-dihydro-1*H*-pyrazol-3-one (ABADEO; Potgieter *et al.*, 2011), and a higher limit of 359.0° in {2-[(1,5-dimethyl-2-phenyl-3-oxo-2,3-dihydro-1*H*-pyrazol-4-ylimino)methyl]-phenoxy}-acetic acid methanol hemisolvate (EVILOK; You *et al.*, 2004). In (**I**), the sum of these angles is *ca* 328.8° for atom N4, hence this atom is highly pyramidal (Fig. 1), more so than for the N atoms in ABADEO. The value of *ca* 354.9° for atom N2 is close to the value of 359.0° observed in EVILOK.

Using the CSD Python API, molecular similarity, only one compound was found when compared to the structure of compound (**I**), namely 1,5-dimethyl-2-phenyl-4-[(1*H*-pyrrol-2-yl-methylene)amino]pyrazol-3(2*H*)-one (DEXTAC; Jing & Chen, 2007), which has a similarity index of 0.726. The structural overlap of the two compounds is shown in Fig. 4; the

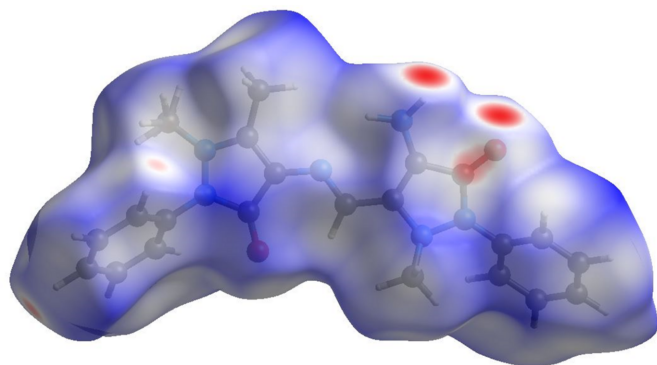


Figure 5
The Hirshfeld surface of (**I**), mapped over d_{norm} .

r.m.s. deviation is 0.018 Å (*Mercury*; Macrae *et al.*, 2020). Here, the —N=C— bond length is 1.282 (1) Å and the dihedral angle involving the phenyl ring and the mean plane of the pyrazole ring is 62.5 (1)°.

5. Hirshfeld surface analysis and two-dimensional fingerprint plots

The Hirshfeld surface analysis and the associated two-dimensional fingerprint plots were generated with *CrystalExplorer17* (Spackman *et al.*, 2021) and interpreted following the protocol of Tan *et al.* (2019). The Hirshfeld surface for compound (**I**) is illustrated in Fig. 5. The presence of prominent red spots indicates that short contacts are particularly significant in the crystal packing.

The full two-dimensional fingerprint plots for (**I**) are given in Fig. 6. The $\text{H}\cdots\text{H}$ contacts have a major contribution of 52.4% to the Hirshfeld surface. The second most significant contribution is from the $\text{C}\cdots\text{H}/\text{H}\cdots\text{C}$ contacts at 23.3%. The $\text{O}\cdots\text{H}/\text{H}\cdots\text{O}$ contacts contribute 12.7% and have sharp pincer-like spikes at $d_e + d_i \simeq 2.1$ Å. The $\text{N}\cdots\text{H}/\text{H}\cdots\text{N}$ contacts contribute 7.0%, and the $\text{C}\cdots\text{C}$ contacts contribute 2.6%. These values can be correlated with the various

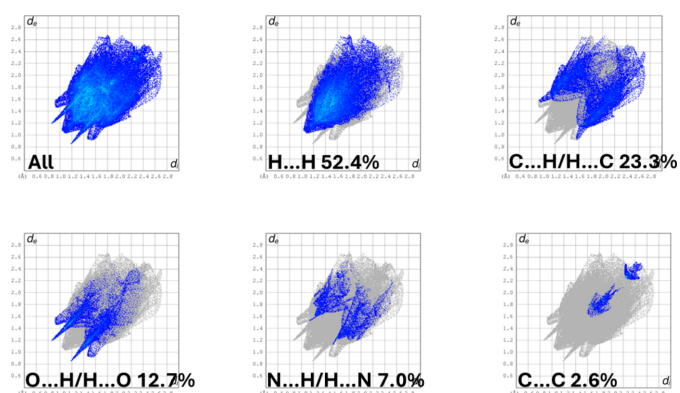


Figure 6
The full two-dimensional fingerprint plot for (**I**), and those delineated into $\text{H}\cdots\text{H}$, $\text{C}\cdots\text{H}/\text{H}\cdots\text{C}$, $\text{O}\cdots\text{H}/\text{H}\cdots\text{O}$, $\text{N}\cdots\text{H}/\text{H}\cdots\text{N}$ and $\text{C}\cdots\text{C}$ contacts.

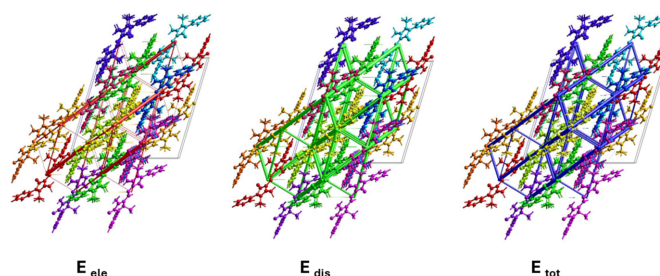


Figure 7
The energy frameworks calculated for (**I**), viewed along the b -axis direction, showing the electrostatic potential forces (E_{ele}), the dispersion forces (E_{dis}) and the total energy diagram (E_{tot}).

hydrogen bonds and other interatomic interactions in the crystal (Table 1).

6. Energy frameworks

A comparison of the energy frameworks calculated for (**I**), showing the electrostatic potential forces (E_{ele}), the dispersion forces (E_{dis}) and the total energy diagrams (E_{tot}), are shown in Fig. 7. The energies were obtained by using wave functions at the HF/3-21G level of theory. The cylindrical radii are proportional to the relative strength of the corresponding energies (Spackman *et al.*, 2021; Tan *et al.*, 2019). They have been adjusted to the same scale factor of 90 with a cut-off value of 6 kJ mol⁻¹ within a radius of 3.8 Å of a central reference molecule.

The major contribution to the intermolecular interactions is from dispersion forces (E_{dis}), as expected in view of the significant contribution to the HS of the $\text{H}\cdots\text{H}$ contacts at 52.4%. The colour-coded interaction mapping within a radius of 3.8 Å of a central reference molecule and the various contributions to the total energy (E_{tot}) for compound (**I**) are given in Fig. S1 of the supporting information.

7. Synthesis, spectroscopic data and thermal analysis

A solution of 0.100 mmol of 4-aminoantipyrene and an equimolar quantity of cadmium chloride (or mercury chloride) in a solvent mixture of 5 ml of methanol and 5 ml of dimethyl formamide (DMF) was refluxed at 363 K for 6 h using an oil bath. The solution was then left at room temperature for 10 days. On evaporation of the solvents reddish-brown crystals of (**I**) were obtained; m.p. 517–518 K. The same compound was obtained when 4-aminoantipyrene was refluxed in methanol and DMF in the absence of the metal chloride. When 4-aminoantipyrene was heated in a mixture of different solvents, it was observed that compound (**I**) was only produced in the presence of DMF.

The absorption spectrum of (**I**) was measured using a UV-Vis spectrometer in the wavelength range of 200–800 nm in CHCl_3 as solvent (Fig. 8a). The absorption band at 258 nm is attributed to the $\pi\text{--}\pi^*$ transitions of the aromatic rings. The second absorption band at 397 nm is due to $n\text{--}\pi^*$ transitions of the C=O and C=N bonds.

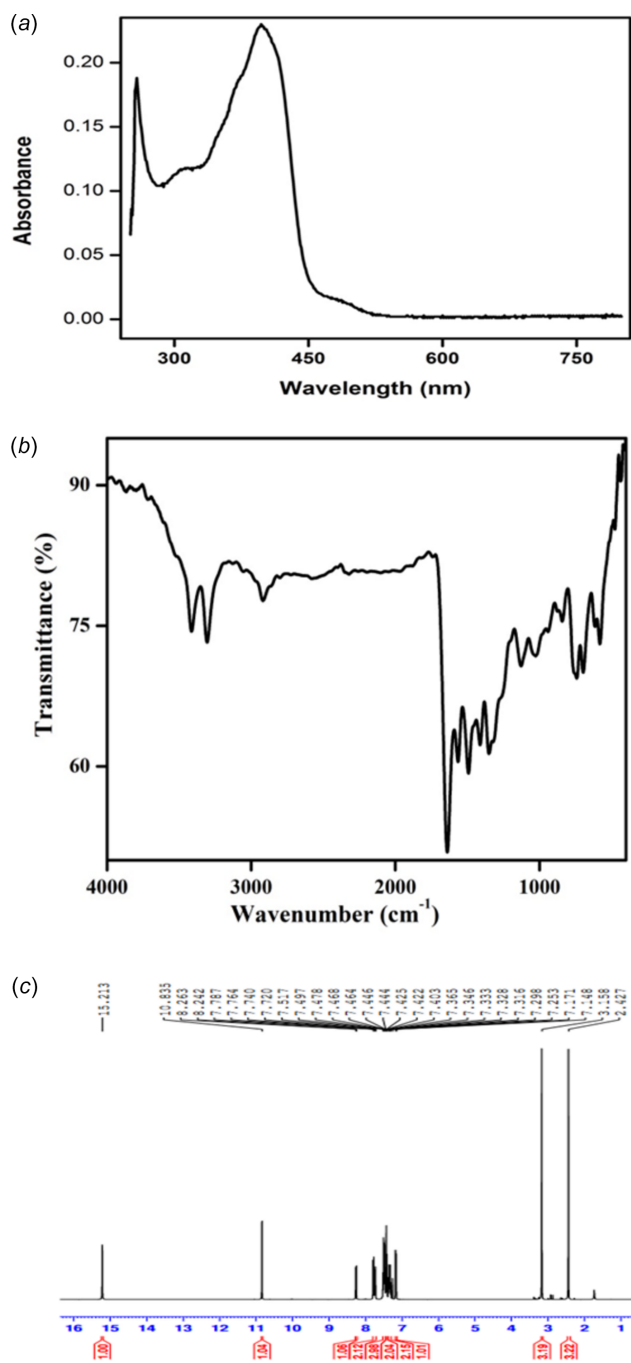


Figure 8
 (a) The UV-vis spectrum of **(I)** in the range 250–800 nm, (b) the FTIR spectrum of **(I)** in the range 400–4000 cm⁻¹, and (c) the ¹H NMR spectrum of **(I)**.

The FTIR spectrum of **(I)** was recorded using a JASCO Infrared spectrometer (KBr pellet) between 400–4000 cm⁻¹ (Fig. 8b). For the spectrum of 4-aminoantipyrene, see Swaminathan *et al.* (2009). A prominent absorption peak at 1569 cm⁻¹ corresponding to the C=N stretching frequency confirms the formation of the Schiff base compound **(I)**. For the NH₂ group of 4-aminoantipyrene, strong symmetric and asymmetric stretching vibrations are observed at 3326 and 3432 cm⁻¹. In compound **(I)**, these vibrations are displaced

Table 2
 Experimental details.

Crystal data	
Chemical formula	C ₂₂ H ₂₂ N ₆ O ₂
<i>M_r</i>	402.45
Crystal system, space group	Monoclinic, C2/c
Temperature (K)	95
<i>a</i> , <i>b</i> , <i>c</i> (Å)	20.2393 (11), 10.6519 (8), 19.4225 (11)
β (°)	106.614 (5)
<i>V</i> (Å ³)	4012.4 (4)
<i>Z</i>	8
Radiation type	Cu Kα
μ (mm ⁻¹)	0.73
Crystal size (mm)	0.11 × 0.06 × 0.02
Data collection	
Diffractometer	SuperNova, Dual, Cu at home/ near, AtlasS2
Absorption correction	Multi-scan (<i>CrysAlis PRO</i> ; Rigaku OD, 2020)
<i>T_{min}</i> , <i>T_{max}</i>	0.489, 1.000
No. of measured, independent and observed [<i>I</i> > 2σ(<i>I</i>)] reflections	11696, 3915, 2695
<i>R_{int}</i>	0.078
(sin θ/λ) _{max} (Å ⁻¹)	0.621
Refinement	
<i>R</i> [<i>F</i> ² > 2σ(<i>F</i> ²)], <i>wR</i> (<i>F</i> ²), <i>S</i>	0.058, 0.137, 1.09
No. of reflections	3915
No. of parameters	281
No. of restraints	3
H-atom treatment	H atoms treated by a mixture of independent and constrained refinement
Δρ _{max} , Δρ _{min} (e Å ⁻³)	0.23, -0.24

Computer programs: *CrysAlis PRO* (Rigaku OD, 2020), *SUPERFLIP* (Palatinus & Chapuis, 2007; *JANA2020* (Petříček *et al.*, 2023), *SHELXL2019/3* (Sheldrick, 2015), *Mercury* (Macrae *et al.*, 2020), *PLATON* (Spek, 2020) and *pubCIF* (Westrip, 2010).

and appear as medium-sized peaks at 3313 and 3421 cm⁻¹. The C=O stretching frequency for 4-aminoantipyrene appears at 1679 cm⁻¹, while for compound **(I)** this vibrational frequency is red shifted to 1648 cm⁻¹. The shifts in the N–H and C=O stretching frequencies suggest a significant conjugation between these functional groups.

The ¹H NMR spectrum of **(I)** was recorded in CDCl₃ using a Bruker AC 400 MHz-NMR spectrometer (Fig. 8c). The peaks at 2.43 ppm and 3.15 ppm correspond to the methyl groups (–CH₃) attached to the carbon and nitrogen atoms, respectively, of the pyrazole rings. The aromatic protons appear in their usual range of 7.15–7.8 ppm, while the methine H atom (H12) resonates at 8.25 ppm confirming the Schiff base formation. As shown by Hansen & Spanget-Larsen (2017), the presence of intramolecular hydrogen bonding has a significant effect on the chemical shifts of the H atoms involved. The presence of the strong intramolecular N–H···N hydrogen bond (N6–H6A···N3) results in a shift to 15.22 ppm for this N–H proton. The resonance at 10.83 ppm can be assigned to the second H atom of the NH₂ group.

An SQT Q600 V20.9 Build 20 Simultaneous Thermo Analytical system was used to measure the TGA/DTA of **(I)** in a nitrogen atmosphere with a heating rate of 10°C min⁻¹ (Fig. S2 of the supporting information). The TGA curve for **(I)** reveals a single-stage weight loss starting around 136°C. The

compound decomposes before reaching its melting point as indicated by the DTA curve.

8. Refinement

Crystal data, data collection and structure refinement details are summarized in Table 2. The amino H atoms (NH₂) were located in a difference-Fourier map and freely refined. The C-bound H atoms were included in calculated positions and refined as riding, with C–H = 0.95–0.98 Å and $U_{\text{iso}}(\text{H}) = 1.2U_{\text{eq}}(\text{C})$ or $1.5U_{\text{eq}}(\text{methyl C})$. The H atoms of methyl group C10 were modelled as disordered over two orientations with an AFIX 123 constraint in *SHELXL*.

Acknowledgements

AS thanks Professor K. Panchanatheswaran, Former Professor, Department of Chemistry, Bharathidasan University, Tiruchirappalli-24, and Dr P. Venkatesan, Assistant Professor of Chemistry, Srimad Andavan Arts and Science College (A), Tiruchirappalli-5, for many fruitful discussions. MK and MD acknowledge using the CzechNanoLab Research Infrastructure supported by MEYS CR (No. LM2018110) for crystallographic analysis. HSE is grateful to the University of Neuchâtel for their support over the years.

References

- Groom, C. R., Bruno, I. J., Lightfoot, M. P. & Ward, S. C. (2016). *Acta Cryst.* **B72**, 171–179.
- Hansen, P. E. & Spanget-Larsen, J. (2017). *Molecules* **22**, 552–572.
- Heravi, M. M., Ghavidel, M. & Mohammadkhani, L. (2018). *RSC Adv.* **8**, 27832–27862.
- Jing, Z.-L. & Chen, X. (2007). *Acta Cryst.* **E63**, o687–o688.
- Kametani, T., Kigasawa, K., Ikari, N., Iwata, T., Saito, M. & Yagi, H. (1967). *Chem. Pharm. Bull.* **15**, 1305–1309.
- Li, Y., Liu, Y., Wang, H., Xiong, X., Wei, P. & Li, F. (2013). *Molecules* **18**, 877–893.
- Loukopoulos, E., Berkoff, B., Griffiths, K., Keeble, V., Dokorou, V. N., Tsipis, A. C., Escuer, A. & Kostakis, G. E. (2015). *CrysiEngComm* **17**, 6753–6764.
- Macrae, C. F., Sovago, I., Cottrell, S. J., Galek, P. T. A., McCabe, P., Pidcock, E., Platings, M., Shields, G. P., Stevens, J. S., Towler, M. & Wood, P. A. (2020). *J. Appl. Cryst.* **53**, 226–235.
- Mnguni, M. J. & Lemmerer, A. (2015). *Acta Cryst.* **C71**, 103–109.
- Palatinus, L. & Chapuis, G. (2007). *J. Appl. Cryst.* **40**, 786–790.
- Parvarinezhad, S., Salehi, M., Kubicki, M. & Eshaghi malekshah, R. (2022). *J. Mol. Struct.* **1260**, 132780.
- Petříček, V., Palatinus, L., Plášil, J. & Dušek, M. (2023). *Z. Kristallogr.* **238**, 271–282.
- Potgieter, K., Hosten, E., Gerber, T. & Betz, R. (2011). *Acta Cryst.* **E67**, o2785–o2786.
- Rigaku OD (2020). *CrysAlis PRO*. Rigaku Oxford Diffraction Ltd., Yarnton, England.
- Sheldrick, G. M. (2015). *Acta Cryst.* **C71**, 3–8.
- Singh, T. P. & Vijayan, M. (1976). *Acta Cryst.* **B32**, 2432–2437.
- Smith, M. G. & Lemmerer, A. (2019). *J. Mol. Struct.* **1175**, 307–313.
- Spackman, P. R., Turner, M. J., McKinnon, J. J., Wolff, S. K., Grimwood, D. J., Jayatilaka, D. & Spackman, M. A. (2021). *J. Appl. Cryst.* **54**, 1006–1011.
- Spek, A. L. (2020). *Acta Cryst.* **E76**, 1–11.
- Stoeckli-Evans, H., Shankar, M. G., Kumaravel, R., Subashini, A., Sabari Girisun, T., Ramamurthi, K., Kučeráková, M., Dušek, M. & Crochet, A. (2025). *Acta Cryst.* **E81** 393–400.
- Swaminathan, J., Ramalingam, M., Sethuraman, V., Sundaraganesan, N. & Sebastian, S. (2009). *Spectrochim. Acta A Mol. Biomol. Spectrosc.* **73**, 593–600.
- Tan, S. L., Jotani, M. M. & Tiekink, E. R. T. (2019). *Acta Cryst.* **E75**, 308–318.
- Vilsmeier, A. & Haack, A. (1927). *Ber. Dtsch. Chem. Ges. A/B* **60**, 119–122.
- Wang, X.-W. & Zheng, Y.-Q. (2007). *Inorg. Chem. Commun.* **10**, 709–712.
- Westrip, S. P. (2010). *J. Appl. Cryst.* **43**, 920–925.
- You, Z.-L., Zhu, H.-L. & Liu, W.-S. (2004). *Acta Cryst.* **E60**, o801–o803.

supporting information

Acta Cryst. (2025). E81, 438-443 [https://doi.org/10.1107/S2056989025003676]

Structure of (*E*)-4-amino-5-[[1,5-dimethyl-3-oxo-2-phenyl-2,3-dihydro-1*H*-pyrazol-4-yl]imino]methyl]-1-methyl-2-phenyl-2,3-dihydro-1*H*-pyrazol-3-one: aerial oxidation of 4-aminoantipyrine in dimethylformamide

R. Kumaravel, Helen Stoeckli-Evans, A. Subashini, M. G. Shankar, Monika Kučeráková, Michal Dušek, Aurélien Crochet and K. Ramamurthi

Computing details

(*E*)-4-Amino-5-[[1,5-dimethyl-3-oxo-2-phenyl-2,3-dihydro-1*H*-pyrazol-4-yl]imino]methyl]-1-methyl-2-phenyl-2,3-dihydro-1*H*-pyrazol-3-one

Crystal data

$C_{22}H_{22}N_6O_2$

$M_r = 402.45$

Monoclinic, *C2/c*

$a = 20.2393$ (11) Å

$b = 10.6519$ (8) Å

$c = 19.4225$ (11) Å

$\beta = 106.614$ (5)°

$V = 4012.4$ (4) Å³

$Z = 8$

$F(000) = 1696$

$D_x = 1.332$ Mg m⁻³

Cu *K* α radiation, $\lambda = 1.54184$ Å

Cell parameters from 2185 reflections

$\theta = 4.5\text{--}73.1^\circ$

$\mu = 0.73$ mm⁻¹

$T = 95$ K

Block, yellow

0.11 × 0.06 × 0.02 mm

Data collection

SuperNova, Dual, Cu at home/near, AtlasS2 diffractometer

Radiation source: micro-focus sealed X-ray tube

Mirror monochromator

Detector resolution: 5.2027 pixels mm⁻¹

ω scans

Absorption correction: multi-scan (CrysAlisPro; Rigaku OD, 2020)

$T_{\min} = 0.489$, $T_{\max} = 1.000$

11696 measured reflections

3915 independent reflections

2695 reflections with $I > 2\sigma(I)$

$R_{\text{int}} = 0.078$

$\theta_{\max} = 73.4^\circ$, $\theta_{\min} = 4.6^\circ$

$h = -20 \rightarrow 24$

$k = -13 \rightarrow 11$

$l = -21 \rightarrow 24$

Refinement

Refinement on F^2

Least-squares matrix: full

$R[F^2 > 2\sigma(F^2)] = 0.058$

$wR(F^2) = 0.137$

$S = 1.09$

3915 reflections

281 parameters

3 restraints

Primary atom site location: structure-invariant direct methods

Secondary atom site location: difference Fourier map

Hydrogen site location: mixed

H atoms treated by a mixture of independent and constrained refinement

$w = 1/[\sigma^2(F_o^2) + (0.0162P)^2 + 0.9186P]$

where $P = (F_o^2 + 2F_c^2)/3$

$(\Delta/\sigma)_{\max} < 0.001$

$\Delta\rho_{\max} = 0.23$ e Å⁻³

$\Delta\rho_{\min} = -0.24$ e Å⁻³

Special details

Geometry. All esds (except the esd in the dihedral angle between two l.s. planes) are estimated using the full covariance matrix. The cell esds are taken into account individually in the estimation of esds in distances, angles and torsion angles; correlations between esds in cell parameters are only used when they are defined by crystal symmetry. An approximate (isotropic) treatment of cell esds is used for estimating esds involving l.s. planes.

Fractional atomic coordinates and isotropic or equivalent isotropic displacement parameters (\AA^2)

	<i>x</i>	<i>y</i>	<i>z</i>	$U_{\text{iso}}^*/U_{\text{eq}}$	Occ. (<1)
O1	0.26471 (10)	0.82349 (18)	0.71602 (11)	0.0333 (5)	
O2	0.48785 (10)	0.67524 (17)	0.45511 (10)	0.0270 (4)	
N1	0.28813 (11)	0.6763 (2)	0.80851 (12)	0.0241 (5)	
N2	0.32274 (11)	0.5621 (2)	0.82181 (12)	0.0239 (5)	
N3	0.36940 (11)	0.6519 (2)	0.66612 (12)	0.0230 (4)	
N4	0.37734 (11)	0.8631 (2)	0.52073 (12)	0.0241 (5)	
N5	0.41266 (11)	0.8324 (2)	0.46958 (12)	0.0225 (5)	
N6	0.45817 (12)	0.5646 (2)	0.58278 (13)	0.0264 (5)	
H6AN	0.4389 (19)	0.534 (4)	0.6156 (19)	0.046 (10)*	
H6BN	0.4769 (18)	0.506 (3)	0.5546 (18)	0.044 (10)*	
C1	0.29526 (13)	0.7285 (2)	0.74460 (15)	0.0252 (5)	
C2	0.34215 (12)	0.6435 (2)	0.72408 (14)	0.0220 (5)	
C3	0.35728 (13)	0.5455 (2)	0.77250 (14)	0.0234 (5)	
C4	0.23438 (14)	0.7031 (3)	0.84031 (14)	0.0258 (5)	
C5	0.23232 (13)	0.8209 (3)	0.86942 (15)	0.0269 (6)	
H5	0.265495	0.882624	0.867108	0.032*	
C6	0.18129 (15)	0.8482 (3)	0.90208 (15)	0.0316 (6)	
H6	0.179484	0.929006	0.922122	0.038*	
C7	0.13298 (14)	0.7580 (3)	0.90557 (16)	0.0314 (6)	
H7	0.098412	0.776905	0.928336	0.038*	
C8	0.13510 (15)	0.6400 (3)	0.87575 (17)	0.0352 (7)	
H8	0.101978	0.578122	0.878016	0.042*	
C9	0.18632 (14)	0.6126 (3)	0.84232 (16)	0.0313 (6)	
H9	0.187874	0.532522	0.821286	0.038*	
C10	0.34044 (15)	0.5069 (3)	0.89333 (14)	0.0300 (6)	
H10A	0.306959	0.534045	0.918095	0.045*	0.5
H10B	0.339565	0.415177	0.889350	0.045*	0.5
H10C	0.386706	0.534382	0.920692	0.045*	0.5
H10D	0.381861	0.455024	0.900663	0.045*	0.5
H10E	0.349255	0.573892	0.929408	0.045*	0.5
H10F	0.302114	0.454687	0.898065	0.045*	0.5
C11	0.40348 (15)	0.4365 (3)	0.77530 (15)	0.0290 (6)	
H11A	0.427737	0.446143	0.738586	0.043*	
H11B	0.376096	0.359208	0.766291	0.043*	
H11C	0.437139	0.432114	0.822884	0.043*	
C12	0.35777 (13)	0.7508 (2)	0.62549 (14)	0.0222 (5)	
H12	0.330612	0.818076	0.634577	0.027*	
C13	0.38717 (13)	0.7557 (2)	0.56620 (14)	0.0237 (5)	
C14	0.42913 (13)	0.6708 (2)	0.54780 (13)	0.0212 (5)	

C15	0.44761 (13)	0.7201 (2)	0.48601 (14)	0.0236 (5)
C16	0.42297 (13)	0.9285 (2)	0.42269 (14)	0.0239 (5)
C17	0.43325 (16)	0.8949 (3)	0.35769 (15)	0.0341 (6)
H17	0.433488	0.809000	0.344528	0.041*
C18	0.44319 (18)	0.9885 (3)	0.31212 (17)	0.0408 (7)
H18	0.450361	0.966070	0.267463	0.049*
C19	0.44287 (15)	1.1135 (3)	0.33029 (17)	0.0343 (7)
H19	0.450448	1.176686	0.298891	0.041*
C20	0.43135 (14)	1.1456 (3)	0.39494 (15)	0.0283 (6)
H20	0.429285	1.231722	0.406967	0.034*
C21	0.42279 (13)	1.0542 (2)	0.44233 (14)	0.0252 (5)
H21	0.416884	1.076869	0.487512	0.030*
C22	0.30443 (14)	0.8929 (3)	0.48461 (18)	0.0376 (7)
H22A	0.279979	0.907024	0.520799	0.056*
H22B	0.283073	0.822685	0.453602	0.056*
H22C	0.301822	0.968835	0.455445	0.056*

Atomic displacement parameters (Å²)

	U^{11}	U^{22}	U^{33}	U^{12}	U^{13}	U^{23}
O1	0.0366 (11)	0.0269 (10)	0.0438 (12)	0.0139 (8)	0.0232 (9)	0.0129 (9)
O2	0.0314 (10)	0.0231 (9)	0.0313 (10)	0.0013 (7)	0.0166 (8)	-0.0011 (7)
N1	0.0262 (11)	0.0212 (10)	0.0297 (12)	0.0040 (8)	0.0158 (9)	0.0056 (9)
N2	0.0259 (11)	0.0212 (10)	0.0268 (11)	0.0024 (8)	0.0112 (9)	0.0030 (9)
N3	0.0220 (10)	0.0235 (10)	0.0257 (11)	0.0008 (8)	0.0104 (9)	0.0009 (9)
N4	0.0247 (11)	0.0252 (11)	0.0271 (12)	0.0037 (8)	0.0147 (9)	0.0036 (9)
N5	0.0257 (11)	0.0219 (10)	0.0229 (11)	0.0015 (8)	0.0117 (9)	0.0014 (8)
N6	0.0336 (12)	0.0194 (11)	0.0300 (13)	0.0049 (9)	0.0150 (10)	0.0034 (9)
C1	0.0249 (13)	0.0262 (13)	0.0279 (13)	0.0016 (10)	0.0131 (11)	0.0021 (11)
C2	0.0205 (12)	0.0208 (11)	0.0276 (13)	0.0023 (9)	0.0113 (10)	0.0024 (10)
C3	0.0234 (12)	0.0233 (12)	0.0242 (13)	0.0000 (10)	0.0082 (10)	-0.0012 (10)
C4	0.0272 (13)	0.0274 (13)	0.0258 (13)	0.0016 (10)	0.0126 (11)	0.0014 (11)
C5	0.0231 (13)	0.0290 (14)	0.0306 (14)	-0.0025 (10)	0.0108 (11)	-0.0052 (11)
C6	0.0340 (15)	0.0327 (15)	0.0297 (15)	0.0031 (12)	0.0117 (12)	-0.0034 (12)
C7	0.0304 (14)	0.0352 (15)	0.0350 (15)	0.0070 (12)	0.0194 (12)	0.0056 (12)
C8	0.0344 (16)	0.0348 (15)	0.0440 (18)	-0.0013 (12)	0.0237 (14)	0.0041 (13)
C9	0.0316 (14)	0.0259 (13)	0.0420 (17)	0.0008 (11)	0.0192 (13)	0.0010 (12)
C10	0.0331 (15)	0.0333 (15)	0.0265 (14)	0.0036 (11)	0.0132 (12)	0.0065 (11)
C11	0.0334 (14)	0.0288 (14)	0.0264 (14)	0.0073 (11)	0.0110 (11)	0.0005 (11)
C12	0.0230 (12)	0.0204 (12)	0.0260 (13)	0.0014 (9)	0.0113 (10)	0.0006 (10)
C13	0.0231 (12)	0.0222 (12)	0.0273 (13)	0.0022 (10)	0.0098 (10)	0.0028 (10)
C14	0.0211 (12)	0.0209 (12)	0.0228 (12)	-0.0015 (9)	0.0081 (10)	-0.0019 (9)
C15	0.0248 (13)	0.0211 (12)	0.0269 (13)	-0.0019 (10)	0.0107 (10)	-0.0018 (10)
C16	0.0237 (12)	0.0245 (13)	0.0246 (13)	-0.0033 (10)	0.0087 (10)	0.0021 (10)
C17	0.0455 (17)	0.0323 (15)	0.0263 (14)	-0.0004 (13)	0.0129 (13)	-0.0022 (12)
C18	0.0512 (19)	0.0448 (18)	0.0308 (15)	-0.0003 (14)	0.0188 (14)	0.0052 (13)
C19	0.0315 (14)	0.0362 (15)	0.0371 (16)	0.0011 (12)	0.0129 (12)	0.0131 (13)
C20	0.0258 (13)	0.0241 (13)	0.0343 (15)	-0.0009 (10)	0.0075 (11)	0.0060 (11)

C21	0.0217 (12)	0.0269 (13)	0.0260 (13)	0.0013 (10)	0.0054 (11)	0.0016 (10)
C22	0.0264 (14)	0.0427 (17)	0.0475 (19)	0.0063 (12)	0.0169 (13)	0.0162 (14)

Geometric parameters (Å, °)

O1—C1	1.232 (3)	C8—H8	0.9500
O2—C15	1.237 (3)	C9—H9	0.9500
N1—N2	1.390 (3)	C10—H10A	0.9800
N1—C1	1.405 (3)	C10—H10B	0.9800
N1—C4	1.425 (3)	C10—H10C	0.9800
N2—C3	1.349 (4)	C10—H10D	0.9800
N2—C10	1.455 (3)	C10—H10E	0.9800
N3—C12	1.297 (3)	C10—H10F	0.9800
N3—C2	1.391 (3)	C11—H11A	0.9800
N4—N5	1.418 (3)	C11—H11B	0.9800
N4—C13	1.424 (3)	C11—H11C	0.9800
N4—C22	1.476 (3)	C12—C13	1.441 (4)
N5—C15	1.379 (3)	C12—H12	0.9500
N5—C16	1.425 (3)	C13—C14	1.357 (4)
N6—C14	1.364 (3)	C14—C15	1.454 (4)
N6—H6AN	0.90 (4)	C16—C17	1.384 (4)
N6—H6BN	0.98 (4)	C16—C21	1.393 (4)
C1—C2	1.447 (4)	C17—C18	1.386 (4)
C2—C3	1.379 (4)	C17—H17	0.9500
C3—C11	1.482 (4)	C18—C19	1.378 (5)
C4—C9	1.378 (4)	C18—H18	0.9500
C4—C5	1.382 (4)	C19—C20	1.384 (4)
C5—C6	1.389 (4)	C19—H19	0.9500
C5—H5	0.9500	C20—C21	1.385 (4)
C6—C7	1.386 (4)	C20—H20	0.9500
C6—H6	0.9500	C21—H21	0.9500
C7—C8	1.390 (4)	C22—H22A	0.9800
C7—H7	0.9500	C22—H22B	0.9800
C8—C9	1.402 (4)	C22—H22C	0.9800
N2—N1—C1	109.7 (2)	H10A—C10—H10C	109.5
N2—N1—C4	120.1 (2)	H10B—C10—H10C	109.5
C1—N1—C4	126.0 (2)	H10D—C10—H10E	109.5
C3—N2—N1	108.5 (2)	H10D—C10—H10F	109.5
C3—N2—C10	126.1 (2)	H10E—C10—H10F	109.5
N1—N2—C10	120.3 (2)	C3—C11—H11A	109.5
C12—N3—C2	120.0 (2)	C3—C11—H11B	109.5
N5—N4—C13	103.86 (19)	H11A—C11—H11B	109.5
N5—N4—C22	110.6 (2)	C3—C11—H11C	109.5
C13—N4—C22	114.3 (2)	H11A—C11—H11C	109.5
C15—N5—N4	111.5 (2)	H11B—C11—H11C	109.5
C15—N5—C16	127.7 (2)	N3—C12—C13	118.1 (2)
N4—N5—C16	118.5 (2)	N3—C12—H12	120.9

C14—N6—H6AN	116 (2)	C13—C12—H12	120.9
C14—N6—H6BN	116 (2)	C14—C13—N4	111.0 (2)
H6AN—N6—H6BN	119 (3)	C14—C13—C12	128.2 (2)
O1—C1—N1	123.9 (2)	N4—C13—C12	120.6 (2)
O1—C1—C2	132.3 (3)	C13—C14—N6	129.4 (3)
N1—C1—C2	103.7 (2)	C13—C14—C15	107.8 (2)
C3—C2—N3	122.6 (2)	N6—C14—C15	122.4 (2)
C3—C2—C1	108.7 (2)	O2—C15—N5	126.0 (2)
N3—C2—C1	128.7 (2)	O2—C15—C14	128.4 (2)
N2—C3—C2	109.0 (2)	N5—C15—C14	105.5 (2)
N2—C3—C11	121.7 (2)	C17—C16—C21	120.8 (3)
C2—C3—C11	129.3 (3)	C17—C16—N5	119.0 (2)
C9—C4—C5	121.3 (3)	C21—C16—N5	120.2 (2)
C9—C4—N1	120.3 (2)	C16—C17—C18	118.9 (3)
C5—C4—N1	118.4 (2)	C16—C17—H17	120.5
C4—C5—C6	119.4 (3)	C18—C17—H17	120.5
C4—C5—H5	120.3	C19—C18—C17	121.3 (3)
C6—C5—H5	120.3	C19—C18—H18	119.3
C7—C6—C5	120.3 (3)	C17—C18—H18	119.3
C7—C6—H6	119.8	C18—C19—C20	119.1 (3)
C5—C6—H6	119.8	C18—C19—H19	120.5
C6—C7—C8	120.0 (3)	C20—C19—H19	120.5
C6—C7—H7	120.0	C19—C20—C21	121.0 (3)
C8—C7—H7	120.0	C19—C20—H20	119.5
C7—C8—C9	119.7 (3)	C21—C20—H20	119.5
C7—C8—H8	120.1	C20—C21—C16	118.9 (3)
C9—C8—H8	120.1	C20—C21—H21	120.5
C4—C9—C8	119.3 (3)	C16—C21—H21	120.5
C4—C9—H9	120.4	N4—C22—H22A	109.5
C8—C9—H9	120.4	N4—C22—H22B	109.5
N2—C10—H10A	109.5	H22A—C22—H22B	109.5
N2—C10—H10B	109.5	N4—C22—H22C	109.5
H10A—C10—H10B	109.5	H22A—C22—H22C	109.5
N2—C10—H10C	109.5	H22B—C22—H22C	109.5
C1—N1—N2—C3	5.9 (3)	C5—C4—C9—C8	-1.2 (4)
C4—N1—N2—C3	164.2 (2)	N1—C4—C9—C8	178.2 (3)
C1—N1—N2—C10	162.1 (2)	C7—C8—C9—C4	0.7 (5)
C4—N1—N2—C10	-39.7 (3)	C2—N3—C12—C13	179.8 (2)
C13—N4—N5—C15	-5.6 (3)	N5—N4—C13—C14	4.3 (3)
C22—N4—N5—C15	-128.7 (2)	C22—N4—C13—C14	124.9 (3)
C13—N4—N5—C16	-169.6 (2)	N5—N4—C13—C12	-179.4 (2)
C22—N4—N5—C16	67.3 (3)	C22—N4—C13—C12	-58.8 (3)
N2—N1—C1—O1	173.0 (3)	N3—C12—C13—C14	-3.0 (4)
C4—N1—C1—O1	16.3 (4)	N3—C12—C13—N4	-178.6 (2)
N2—N1—C1—C2	-5.3 (3)	N4—C13—C14—N6	170.8 (3)
C4—N1—C1—C2	-162.0 (2)	C12—C13—C14—N6	-5.2 (5)
C12—N3—C2—C3	-174.6 (2)	N4—C13—C14—C15	-1.5 (3)

C12—N3—C2—C1	5.8 (4)	C12—C13—C14—C15	-177.4 (3)
O1—C1—C2—C3	-175.1 (3)	N4—N5—C15—O2	-172.9 (2)
N1—C1—C2—C3	2.9 (3)	C16—N5—C15—O2	-10.8 (4)
O1—C1—C2—N3	4.5 (5)	N4—N5—C15—C14	4.9 (3)
N1—C1—C2—N3	-177.4 (2)	C16—N5—C15—C14	167.0 (2)
N1—N2—C3—C2	-3.9 (3)	C13—C14—C15—O2	175.7 (3)
C10—N2—C3—C2	-158.3 (2)	N6—C14—C15—O2	2.8 (4)
N1—N2—C3—C11	175.5 (2)	C13—C14—C15—N5	-2.0 (3)
C10—N2—C3—C11	21.1 (4)	N6—C14—C15—N5	-174.9 (2)
N3—C2—C3—N2	-179.1 (2)	C15—N5—C16—C17	42.4 (4)
C1—C2—C3—N2	0.5 (3)	N4—N5—C16—C17	-156.5 (2)
N3—C2—C3—C11	1.5 (4)	C15—N5—C16—C21	-137.4 (3)
C1—C2—C3—C11	-178.9 (3)	N4—N5—C16—C21	23.7 (3)
N2—N1—C4—C9	-42.8 (4)	C21—C16—C17—C18	-0.2 (4)
C1—N1—C4—C9	111.6 (3)	N5—C16—C17—C18	179.9 (3)
N2—N1—C4—C5	136.5 (3)	C16—C17—C18—C19	-0.1 (5)
C1—N1—C4—C5	-69.0 (4)	C17—C18—C19—C20	-1.0 (5)
C9—C4—C5—C6	0.7 (4)	C18—C19—C20—C21	2.4 (4)
N1—C4—C5—C6	-178.6 (3)	C19—C20—C21—C16	-2.7 (4)
C4—C5—C6—C7	0.1 (4)	C17—C16—C21—C20	1.6 (4)
C5—C6—C7—C8	-0.5 (4)	N5—C16—C21—C20	-178.5 (2)
C6—C7—C8—C9	0.1 (5)		

Hydrogen-bond geometry (Å, °)

Cg1 is the centroid of C4—C9 phenyl ring.

<i>D</i> —H... <i>A</i>	<i>D</i> —H	H... <i>A</i>	<i>D</i> ... <i>A</i>	<i>D</i> —H... <i>A</i>
N6—H6AN...N3	0.90 (4)	2.30 (4)	2.894 (3)	123 (3)
N6—H6BN...O2 ⁱ	0.98 (3)	2.09 (3)	2.953 (3)	147 (3)
C7—H7...O2 ⁱⁱ	0.95	2.49	3.417 (4)	165
C10—H10D...O2 ⁱⁱⁱ	0.98	2.52	3.472 (4)	164
C12—H12...O1	0.95	2.34	3.022 (3)	128
C17—H17...O2	0.95	2.55	3.013 (4)	110
C11—H11B...Cg1 ⁱⁱⁱ	0.98	2.96	3.645 (3)	128

Symmetry codes: (i) $-x+1, -y+1, -z+1$; (ii) $x-1/2, -y+3/2, z+1/2$; (iii) $x, -y+1, z+1/2$.